Spatially-resolved emission of GaAs/AlGaAs quantum dots grown by nanohole-filled droplet epitaxy

Ekaterina I. Deribina ⓘ,[*] Aleksei O. Murzin ⓘ, Elena A. Bashegurova ⓘ, Anna Yu. Samsonova, Maksim S. Lozhkin,
Vyacheslav A. Lovcjus ⓘ, Sergey A. Eliseev, Yury P. Efimov, and Yury V. Kapitonov

Department of Photonics, Saint Petersburg State University, Ulyanovskaya d.1, Saint Petersburg 198504, Russia

GaAs/AlGaAs quantum dots created by the nanohole-filling droplet epitaxy are promising for applications in information photonics due to the low mechanical stress in these lattice-matched heterostructures. In this work, we have carried out a detailed study of the optical properties of such quantum dots using microphotoluminescence and reflection spectroscopy. For quantum dots grown by molecular beam epitaxy with a density of about $1\ \mu m^{-2}$, the photoluminescence signal was scanned with a spatial resolution of about 1 μm. A correlation map was constructed for the spatial derivatives of the photoluminescence spectra in order to identify the emission bands that correlate with each other. It was found that QD A ($E = 1.56$ eV), QD B1 ($E = 1.61$ eV), and QD B2 ($E = 1.65$ eV) bands originate from the same regions of the sample. The smaller width and the lower energy position of the QD A band allow it to be related to the central part of the quantum dot, while the QD B1 and the QD B2 bands' origins are smaller quantum-sized objects located around the same dot. All these bands are observed in anticorrelation with the signal from the heavy-hole exciton in the quantum well.

I. INTRODUCTION

The quantum confinement of charge carriers in quantum dots (QDs) allows them to be used in many photonics applications ranging from lasers [1] to single photon sources [2]. The traditional method for creating AIIIBV semiconductor QDs is the lattice-mismatched growth of InAs on GaAs [3]. Strain in self-organized InAs-based QDs creates electric field gradients that enable interactions with nuclear spins, which is the main source of the electron spin decoherence [4]. Engineering QDs with reduced strain is therefore important for applications requiring long spin relaxation times [5–8].

An alternative approach is the growth of QDs using droplet epitaxy. This method is based on the fact that droplets of gallium self-organize on the surface of GaAs or AlGaAs in the case of an insufficient amount of arsenic. The surface density of the droplets formed can be controlled using the substrate temperature over a wide 10^8–10^{11} cm^{-2} range [9]. The simplest strategy is the further conversion of droplets of gallium into GaAs by turning on the flow of arsenic and covering the resulting nanocrystals with a AlGaAs barrier layer [10]. Despite the rich possibilities for controlling the shape and arrangement of such QDs [11–13], the optical quality of the obtained structures is quite low, which is due to the low temperature of Ga droplet conversion into GaAs (usually around 200 °C). To obtain emission from such structures, rapid thermal annealing (RTA) is necessary, which increases the inhomogeneity of the QDs ensemble.

A breakthrough in the application of droplet epitaxy was the discovery of local droplet etching [14]. In this mode of epitaxy, as the substrate temperature rises above 500 °C [9,15,16], nanoholes are etched under Ga droplets. Further, these nanoholes can be filled with barrier layers and dot material between them to obtain GaAs/AlGaAs QDs [17]. This method is called nanohole-filled droplet epitaxy (NFDE). The optimal GaAs growth temperature makes these QDs defect-free without the need for RTA. Partial filling of the nanoholes leads to high homogeneity of QDs ensembles. Temperature control during the formation of Ga droplets is used to obtain the desired density of QDs to satisfy a wide variety of applications requiring either the addressing of single QDs or the presence of dense QD ensembles.

In many works, single NFDE QDs have been studied, including their fine-structure splitting [18–20] and magneto-optical properties [21,22]. However, the study of the emission spectra from large areas of the sample with a large number of QDs revealed the presence of two or more emission bands with a separation of several tens of meV [19,23]. The presence of two bands can be associated both with two QD subensembles and with the presence of several quantization regions at one dot. A magnetophotoluminescence study [23] put forward a hypothesis that the observed QD A ($E = 1.58$ eV) and QD B ($E = 1.63$ eV) bands correspond to the dot inside the nanohole and additional dots formed on the border of the nanohole.

In our work, we scanned the microphotoluminescence signal, collecting data on several hundreds of single QDs. The data obtained were used to build a correlation map that unambiguously indicates the correlation or anticorrelation of individual emission bands. The temperature-dependent photoluminescence (PL) was studied for these bands, and the positions of the resonances of heavy-hole (HH) and light-hole (LH) excitons in the quantum well (QW) lying between QDs were determined using reflection spectroscopy.
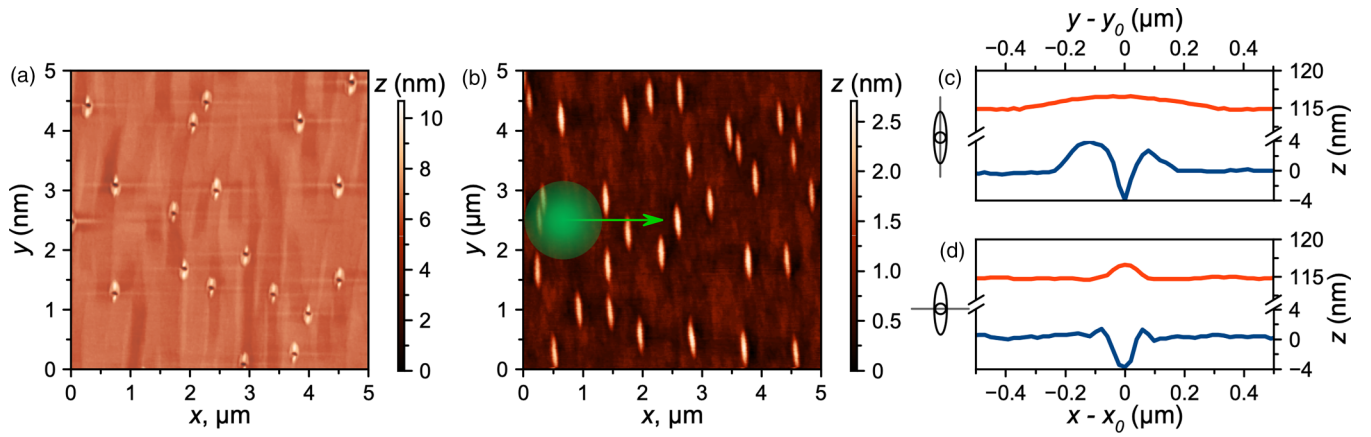
[*]e.deribina@spbu.ru

FIG. 1. AFM images of the sample with nanoholes (a) and with QDs (b). The green circle denotes the approximate size of the laser spot. AFM profiles of nanoholes (blue) and QDs (red) along the [$\bar{1}$10] (c) and [110] (d) directions.

II. SAMPLE GROWTH AND CHARACTERIZATION

The sample (T874) was grown on epi-ready GaAs (001) substrate using the SVTA MBE-35-3 molecular beam epitaxy setup. The substrate was kept at 510 °C during the growth. A 200-nm GaAs buffer layer was grown. After this all shutters were closed for 30 s to smooth the surface and reduce the As flux. Then the Ga source was opened for a time equal to the growth of 2.8-nm GaAs. The Ga flux corresponded to the growth rate of 0.3 monolayers/s. After this, As flux was supplied to the substrate for 300 s to locally etch nanoholes. Then the sample was covered with a 7.3-nm $Al_{0.47}Ga_{0.53}As$ barrier and a 3.4-nm GaAs layer. Subsequently all shutters were closed for a 120-s pause to smooth the surface and fill nanoholes with GaAs. During the growth pause, a redistribution of GaAs occurs: part of the material deposited near the nanoholes fills them. The resulting cone-shaped GaAs form QDs. In the vicinity of these QDs the GaAs layer is depleted. Far from QDs, the 3.4-nm GaAs layer remains, which leads to formation of a QW. Next the 84-nm $Al_{0.38}Ga_{0.62}As$ barrier and 20-nm GaAs cap layers were grown.

For the analysis of nanoholes, a sample (T873) was grown that was interrupted after the etching step. Surface relief of both samples was studied by atomic force microscopy (AFM) using the NT-MDT Integra microscope.

Figure 1(a) shows the AFM image of the etched sample surface. Nanoholes are visible on the surface, surrounded by raised borders. Such structures are typical for local droplet etching under Ga droplets [14]. An AFM image of the surface after growth of subsequent layers is shown in Fig. 1(a). Hills are formed in place of the nanoholes. The density of obtained QDs is around 1 μm^{-2}. Both holes and hills have an asymmetric shape, which is illustrated by cross sections in Figs. 1(c) and 1(d).

III. OPTICAL STUDY

Micro-PL measurements were carried out at $T = 4$ K using a 532-nm cw laser focused down to an ∼1-μm^2 spot by a 50× microobjective lens. Figure 1(b) shows a typical spot

size in scale. A spectrometer with 750-μeV resolution was used. Micro-PL was scanned by the lens movement along the x direction with sub-micrometer resolution. Reflection measurements were carried out at $T = 10$ K using a halogen lamp in geometry close to the Brewster angle for GaAs (74°) [24]. The signal with P polarization was normalized to the signal with S polarization.

Figure 2(a) shows the PL spectrum averaged over the large area of the sample. The following bands could be distinguished in the spectrum: excitonic emission from the bulk GaAs layer ($E = 1.515$ eV), emission from carbon impurities in GaAs ($E = 1.493$ eV) [25], excitonic emission from the bulk AlGaAs layer ($E = 1.98$ eV, not shown) and three bands related to QDs: QD A ($E = 1.56$ eV), QD B1 ($E = 1.61$ eV), and QD B2 ($E = 1.65$ eV), designated following Ref. [23].

During the sample growth on a part of the surface free of nanoholes, QWs are formed. Due to the large QW area, exciton resonances in QWs have a strong enough oscillator strength to be observed in the reflectivity spectrum. Figure 2(a) shows the reflectivity spectra (blue curve). Two resonances corresponding to the heavy-hole (QW HH, $E = 1.710$ eV) and light-hole (QW LH, $E = 1.750$ eV) excitons in QW are observed. The emission from QW is seen only from the lowest-lying QW HH state ($E = 1.700$ eV). The reflectivity and PL spectra were obtained from different points on the sample, which accounts for the slight variation in observed energies caused by the sample's gradient.

One of the possible explanations for several spectral features in PL spectra is the presence of monolayer fluctuations in the QW. In order to test this hypothesis, the QW emission was modeled using NEXTNANO software [26]. The energy levels of the electron, light, and heavy holes were calculated for a QW with barriers having the same composition as in the T874 sample. The thicknesses of the QW varied from 10 to 20 monolayers of GaAs. The materials' parameters were taken for $T = 4$ K. The difference between first electron and hole levels was taken as the transition energy neglecting the exciton binding energy.

Figure 3 shows the calculated dependency of the QW HH and QW LH resonances' positions on the number of GaAs monolayers (MLs) in the QW. The calculated spectral position
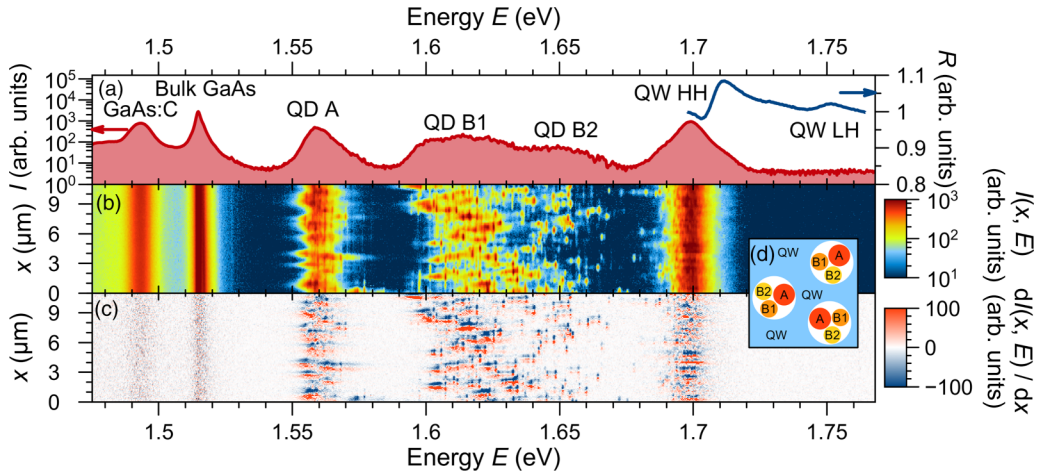
FIG. 2. (a) The averaged PL spectrum ($T = 4$ K, red curve, log scale) and the reflectivity spectrum ($T = 10$ K, blue curve). (b) PL map $I(E, x)$ for the scan along the x direction ($T = 4$ K). Log intensity scale. (c) Spatial derivative $dI(E, x)/dx$ of the PL map in panel (b). (d) Schematic representation of the emitting regions of the sample.

and HH-LH splitting are in good agreement with the experimental values for grown 12-ML QWs. The calculation also predicts monolayer fluctuations of the order of 0.02 eV, which were not observed in the experimental spectra.

In the PL spectrum shown in Fig. 2(a), three bands are identified as QDs emission: QD A ($E = 1.560$ eV), QD B1 ($E = 1.614$ eV), and QD B2 ($E = 1.649$ eV). To establish the nature of these bands, we studied the spatial dependence of the micro-PL spectra. The micro-PL signal was scanned along the x direction—"across" the elongated QDs [scan direction is shown in Fig. 1(b)]. Figure 2(b) shows the spatial dependency of the micro-PL signal. The intensities of bulk GaAs and GaAs:C emission bands remain constant across the sample. Other bands change with the position to some extent. In order to isolate signals from individual QDs and to find the relation

FIG. 3. Calculated transition energies for heavy-hole and light-hole excitons in the $Al_{0.47}Ga_{0.53}As/GaAs/Al_{0.38}Ga_{0.62}As$ quantum well at 4 K for different numbers of GaAs monolayers. According to the growth data, the expected thickness of the QW in the studied sample is 12 MLs.

between emission bands, the correlation map was constructed by the following procedure.

First, the spatial derivative of the PL map $I(E, x)$ was calculated as $dI(E, x)/dx$ [Fig. 2(c)]. For the movement along the x direction, the positive derivative values $dI(E, x)/dx > 0$ correspond to the emergence of the emission [red areas in Fig. 2(c)] and the negative derivative values $dI(E, x)/dx < 0$ correspond to the emission disappearance (blue areas). Both absent and constant emissions will result in zero values (white areas).

Subsequently, the autocorrelation maps $C(E_i, E_j, x)$ were constructed for spatial derivative maps at each x position by the following formula:

$$C(E_i, E_j, x) = \frac{dI(E_i, x)}{dx} \frac{dI(E_j, x)}{dx}. \quad (1)$$

Finally, the correlation map $C(E_i, E_j)$ for the entire scanned part of the sample was calculated by averaging of all autocorrelation maps: $C(E_i, E_j) = \langle C(E_i, E_j, x) \rangle_x$. Figure 4 shows the correlation map constructed from the sample scan of 57 μm in the x direction.

The elements on the diagonal of the correlation map ($E_i = E_j$) are the averaged values of the squared spatial derivatives. The nonzero values observed in these diagonal elements correspond to PL bands that exhibit a spatial dependency in their intensity. The correlation map for bulk GaAs and GaAs:C bands exhibits zero values, as their intensity remains independent of the position.

The off-diagonal elements of the map ($E_i \neq E_j$) represent the correlation between the spatial derivatives of the emission bands with energies E_i and E_j.

Three possible scenarios can be observed in the correlation map. Regions where $C(x, E_i, E_j) > 0$ (shown in red in Fig. 4) indicate a correlation between the emission bands with energies E_i and E_j. This implies that their emission simultaneously appears or disappears during the spatial scan. Conversely, regions with negative values $C(x, E_i, E_j) < 0$ (shown in blue) represent an anticorrelation between the bands. In this case, the emergence of one peak coincides with the disappearance of another. Areas with $C(x, E_i, E_j) \approx 0$ (shown in white)
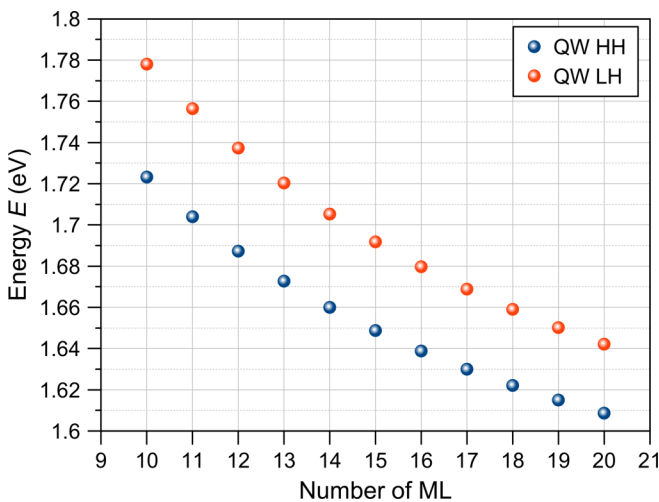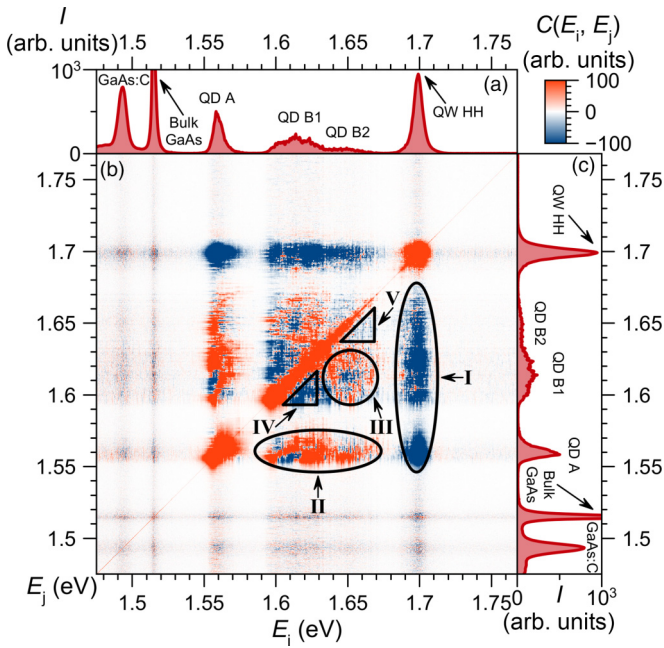
FIG. 4. (a, c) The PL spectrum $I(E)$ averaged along the x axis taken at $T = 4$ K. (b) Correlation map $C(E_i, E_j)$.
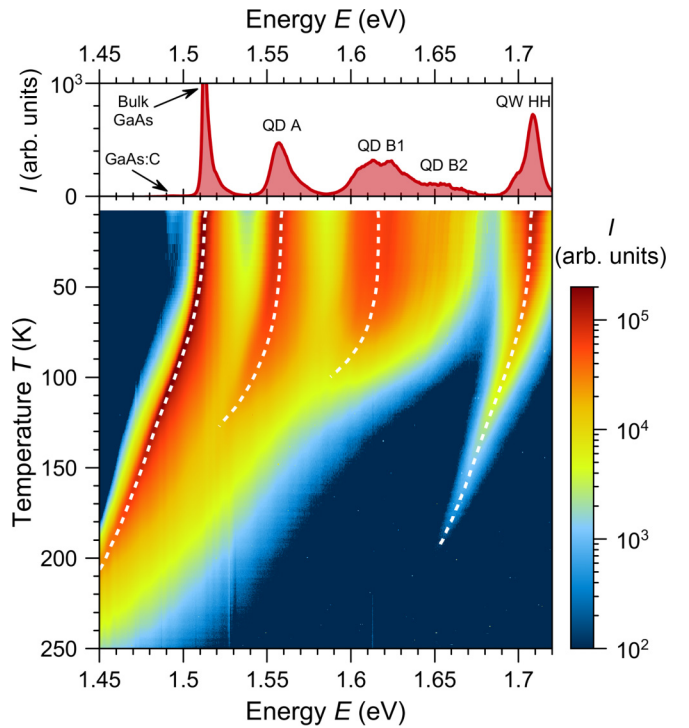

FIG. 5. PL spectra for different sample temperatures (below) and spatially-averaged PL spectrum for $T = 4$ K (above) with PL bands indicated. Log intensity scale.

indicate not only the absence of emission or constant emission but also noncorrelated emissions.

Let us consider the correlation map (Fig. 4) in detail. The QW HH emission shows anticorrelation with all three QD bands (QD A, QD B1, and QD B2; region I in Fig. 4). This observation can be attributed to the presence of a GaAs depletion region surrounding the QDs. The GaAs material fills the nanoholes and forms the QDs during a pause in the epitaxial growth process [27]. As a result, the QW signal is only observed in areas that are distant from the QDs. This phenomenon accounts for the observed anticorrelation between the QDs and the QW bands.

The QD A emission band correlates with QD B1 and QD B2 bands (region II in Fig. 4). This means that all three bands belong to the same QD surroundings and are not the manifestation of three subensembles of QDs. It also aligns with the findings of microscopic measurements depicted in Fig. 1, demonstrating the unimodal size distribution of both etched nanoholes and fully grown hills.

The splitting between the QD A and QD B1 bands, as well as between the QD B1 and QD B2 bands, is around 50 meV. The binding energy of different exciton complexes in NFDE QDs is on the order of a few meV [28–31]. This rules out the possibility that observed emission bands are related to exciton complexes coexisting in the same QD. Thus, these bands correspond to the emission of different quantum-sized objects localized close to each other (at the position of a single nanohole). The QD A emission with the lowest emission energy corresponds to the biggest of the objects. This allows us to consider that the QD A band refers to the GaAs material that filled the nanohole, while the QD B1 and QD B2 bands correspond to other objects that are formed near the nanohole, for example, due to the presence of the elevated border around it. This result supports the same hypothesis drawn in Ref. [23]

based on the magneto-PL study. The QD B1 and QD B2 bands correlate with each other (region III in Fig. 4), which means that all three objects (A, B1, and B2) are usually present together.

The fine structure of the QD B1 band displays an anticorrelation within the band itself, as depicted by region IV in Fig. 4. This behavior can be explained as follows: when examining each individual micro-PL spectrum, only a limited number of narrow QD B1 emission lines are observed. In the presence of one of these lines, the likelihood of observing other lines decreases. Consequently, only several narrow lines are seen for each individual nanohill, but the variation in their positions across different nanohills results in a broad QD B1 band when examining the spatially-averaged PL spectrum [Fig. 2(a)]. A similar observation, though to a lesser extent, can be made for the QD B2 band (region V in Fig. 4). Contrasting to QD B bands, the QD A band is considerably narrower, aligning with its attribution to the emission of the intended NFDE-grown QDs.

The information obtained from analysis of correlation maps is summarized in schematic representation of the emitting regions of the sample in Fig. 2(d). We refrain from explaining the smaller features in Fig. 4 because, unlike those already discussed above, they are not observed in every region of the sample.

Figure 5 shows the temperature dependency of the spatially-averaged PL spectrum. All bands are subject to the red shift with increasing temperature, which could be explained by the decrease of the GaAs band gap. Bulk GaAs emission is observed almost up to room temperature, the QW HH and QD A emission intensity drops around 100 K,

the QD B1 and QD B2 emission at even smaller temperatures. This behavior could be explained by the weaker confining potential for QD B1 and QD B2, leading to the easier thermal escape from these states and quenching of the PL emission with temperature growth.

IV. CONCLUSIONS

In this work, we have studied the micro-PL and reflectivity from GaAs/AlGaAs NFDE QDs. The following emission bands were identified: excitonic and carbon-impurity-related emission in bulk GaAs and heavy-hole exciton emission from the QW formed around QDs and three QD emission bands: QD A, QD B1, and QD B2. To establish the relationship between these bands, we analyzed the correlation between them in a large set of micro-PL spectra obtained by sample scanning. This analysis proved the existence of the region with GaAs depletion resulted in the anticorrelation of QW and QD emissions. The lowest-lying narrow QD A emission band was identified as the emission of the GaAs-filled nanoholes. The QD B1 and QD B2 bands correspond to smaller quantum-sized objects located around the nanohole.

[1] N. N. Ledentsov, Quantum dot laser, Semicond. Sci. Technol. **26**, 014001 (2011).

[2] C. Santori, D. Fattal, J. Vuckovic, G. S. Solomon, and Y. Yamamoto, Single-photon generation with InAs quantum dots, New J. Phys. **6**, 89 (2004).

[3] J. Y. Marzin, J. M. Gérard, A. Izraël, D. Barrier, and G. Bastard, Photoluminescence of single InAs quantum dots obtained by self-organized growth on GaAs, Phys. Rev. Lett. **73**, 716 (1994).

[4] A. Bechtold, D. Rauch, F. Li, T. Simmet, P.-L. Ardelt, A. Regler, K. Müller, N. A. Sinitsyn, and J. J. Finley, Three-stage decoherence dynamics of an electron spin qubit in an optically active quantum dot, Nat. Phys. **11**, 1005 (2015).

[5] L. Langer, S. V. Poltavtsev, I. A. Yugova, M. Salewski, D. R. Yakovlev, G. Karczewski, T. Wojtowicz, I. A. Akimov, and M. Bayer, Access to long-term optical memories using photon echoes retrieved from semiconductor spins, Nat. Photon. **8**, 851 (2014).

[6] S. V. Poltavtsev, L. Langer, I. A. Yugova, M. Salewski, Y. V. Kapitonov, D. R. Yakovlev, G. Karczewski, T. Wojtowicz, I. A. Akimov, and M. Bayer, Access to long-term optical memories using photon echoes retrieved from electron spins in semiconductor quantum wells, Proc. SPIE **9931**, 99311V (2016).

[7] I. A. Solovev, I. I. Yanibekov, Y. P. Efimov, S. A. Eliseev, V. A. Lovcjus, I. A. Yugova, S. V. Poltavtsev, and Y. V. Kapitonov, Long-lived dark coherence brought to light by magnetic-field controlled photon echo, Phys. Rev. B **103**, 235312 (2021).

[8] I. A. Solovev, I. I. Yanibekov, I. A. Babenko, B. V. Stroganov, S. A. Eliseev, V. A. Lovcjus, Y. P. Efimov, S. V. Poltavtsev, Y. V. Kapitonov, and I. A. Yugova, Manipulation of optical coherence of quantum-well excitons by transverse magnetic field, Phys. Rev. B **106**, 115401 (2022).

[9] C. Heyn, Kinetic model of local droplet etching, Phys. Rev. B **83**, 165302 (2011).

[10] K. Watanabe, N. Koguchi, and Y. Gotoh, Fabrication of GaAs quantum dots by modified droplet epitaxy, Jpn. J. Appl. Phys. **39**, L79 (2000).

[11] M. Yamagiwa, N. Sumita, F. Minami, and N. Koguchi, Confined electronic structure in GaAs quantum dots, J. Lumin. **108**, 379 (2004).

[12] T. Mano and N. Koguchi, Nanometer-scale GaAs ring structure grown by droplet epitaxy, J. Cryst. Growth **278**, 108 (2005).

[13] T. Mano, T. Kuroda, M. Yamagiwa, G. Kido, K. Sakoda, and N. Koguchi, Lasing in GaAs/AlGaAs self-assembled quantum dots, Appl. Phys. Lett. **89**, 183102 (2006).

[14] Z. M. Wang, B. L. Liang, K. A. Sablon, and G. J. Salamo, Nanoholes fabricated by self-assembled gallium nanodrill on GaAs(100), Appl. Phys. Lett. **90**, 113120 (2007).

[15] C. Heyn, A. Stemmann, and W. Hansen, Dynamics of self-assembled droplet etching, Appl. Phys. Lett. **95**, 173110 (2009).

[16] C. Heyn, A. Stemmann, and W. Hansen, Nanohole formation on AlGaAs surfaces by local droplet etching with gallium, J. Cryst. Growth **311**, 1839 (2009).

[17] P. Atkinson, E. Zallo, and O. G. Schmidt, Independent wavelength and density control of uniform GaAs/AlGaAs quantum dots grown by infilling self-assembled nanoholes, J. Appl. Phys. **112**, 054303 (2012).

[18] Y. H. Huo, A. Rastelli, and O. G. Schmidt, Ultra-small excitonic fine structure splitting in highly symmetric quantum dots on GaAs (001) substrate, Appl. Phys. Lett. **102**, 152105 (2013).

[19] M. Gong, B. Hofer, E. Zallo, R. Trotta, J.-W. Luo, O. G. Schmidt, and C. Zhang, Statistical properties of exciton fine structure splitting and polarization angles in quantum dot ensembles, Phys. Rev. B **89**, 205312 (2014).

[20] M. Abbarchi, T. Mano, T. Kuroda, A. Ohtake, and K. Sakoda, Polarization anisotropies in strain-free, asymmetric, and symmetric quantum dots grown by droplet epitaxy, Nanomaterials **11**, 443 (2021).

[21] L. Zaporski, N. Shofer, J. H. Bodey, S. Manna, G. Gillard, M. H. Appel, C. Schimpf, S. F. Covre da Silva, J. Jarman, G. Delamare, G. Park, U. Haeusler, E. A. Chekhovich, A. Rastelli, D. A. Gangloff, M. Atatüre, and C. Le Gall, Ideal refocusing of an optically active spin qubit under strong hyperfine interactions, Nat. Nanotechnol. **18**, 257 (2023).

[22] P. Millington-Hotze, S. Manna, S. F. Covre da Silva, A. Rastelli, and E. A. Chekhovich, Nuclear spin diffusion in the central spin system of a GaAs/AlGaAs quantum dot, Nat. Commun. **14**, 2677 (2023).

[23] A. Ulhaq, Q. Duan, E. Zallo, F. Ding, O. G. Schmidt, A. I. Tartakovskii, M. S. Skolnick, and E. A. Chekhovich, Vanishing electron *g* factor and long-lived nuclear spin polarization in weakly strained nanohole-filled GaAs/AlGaAs quantum dots, Phys. Rev. B **93**, 165306 (2016).

[24] S. Poltavtsev, Y. Efimov, Y. Dolgikh, S. Eliseev, V. Petrov, and V. Ovsyankin, Extremely low inhomogeneous broadening of exciton lines in shallow (In,Ga)As/GaAs quantum wells, Solid State Commun. **199**, 47 (2014).

[25] Z. Yang, A. Surrente, G. Tutuncuoglu, K. Galkowski, M. Cazaban-Carrazé, F. Amaduzzi, P. Leroux, D. K. Maude, A. Fontcuberta i Morral, and P. Plochocka, Revealing large-scale homogeneity and trace impurity sensitivity of GaAs nanoscale membranes, Nano Lett. **17**, 2979 (2017).

[26] S. Birner, T. Zibold, T. Andlauer, T. Kubis, M. Sabathil, A. Trellakis, and P. Vogl, nextnano: General purpose 3-D simulations, IEEE Tran. Electron Devices, **54**, 2137 (2007).

[27] M. C. Löbl, L. Zhai, J.-P. Jahn, J. Ritzmann, Y. Huo, A. D. Wieck, O. G. Schmidt, A. Ludwig, A. Rastelli, and R. J. Warburton, Correlations between optical properties and Voronoi-cell area of quantum dots, Phys. Rev. B **100**, 155402 (2019).

[28] Z. Trabelsi, M. Yahyaoui, S. B. Radhia, K. Boujdaria, E. Zallo, O. Schmidt, P. Atkinson, M. Chamarro, and C. Testelin, Neutral, charged excitons and biexcitons in strain-free and asymmetric GaAs quantum dots fabricated by local droplet etching, J. Lumin. **197**, 47 (2018).

[29] S. Germanis, P. Atkinson, R. Hostein, S. Suffit, F. Margaillan, V. Voliotis, and B. Eble, Electrical control of optically pumped electron spin in a single GaAs/AlAs quantum dot fabricated by nanohole infilling, Phys. Rev. B **102**, 035406 (2020).

[30] L. Zhai, M. C. Löbl, G. N. Nguyen, J. Ritzmann, A. Javadi, C. Spinnler, A. D. Wieck, A. Ludwig, and R. J. Warburton, Low-noise GaAs quantum dots for quantum photonics, Nat. Commun. **11**, 4745 (2020).

[31] H. Huang, D. Csontosová, S. Manna, Y. Huo, R. Trotta, A. Rastelli, and P. Klenovský, Electric field induced tuning of electronic correlation in weakly confining quantum dots, Phys. Rev. B **104**, 165401 (2021).